ISBN: 978-3-95450-191-5 doi:10.18429/JACoW-SRF2017-TUPB046

# EXPERIENCE ON DESIGN, FABRICATION AND TESTING OF A LARGE GRAIN ESS MEDIUM BETA PROTOTYPE CAVITY

M. Bertucci†, A. Bignami, A. Bosotti, J.F. Chen, P. Michelato, L. Monaco, R. Paparella, D. Sertore, INFN–LASA, Segrate (MI), Italy
C. Pagani, University of Milano & INFN-LASA, Milano, Italy
S. Pirani*, ESS, Lund, Sweden and on leave at INFN-LASA, Segrate (MI), Italy

*Abstract*

INFN-LASA built a complete Medium Beta cavity, based on the ESS prototype design, with novel large-grain material sliced in sheets from an ingot provided by CBMM manufacturing experience. Design and fabrication are reported as well as results on the physical and chemical analyses performed on samples at different cavity production stages. Results from the cold tests performed are also summarized and critically discussed in view of future R&D activities.

## INTRODUCTION

In the framework of the ESS activity in progress at INFN - LASA, we have designed a 704.42 MHz Medium (β=0.67) beta prototype cavity plug compatible [1] with the ESS cryomodule design [2]. Two prototypes of these cavities have been built and treated at Ettore Zanon S.p.A. under the supervision of INFN-LASA, following a "build-to-print" scheme, namely the same successful strategy adopted for the production of the 800 1.3 GHz and of the 20 3.9 GHz series cavities of the European XFEL [3, 4]. To validate the cavity design and the production process, one cavity (MB001) was built using Fine Grain niobium (i.e. the standard technology), as foreseen for the series. A second prototype (MBLG002) has been produced using Large Grain niobium with the aim of exploring the possibilities and potentialities of this material, exploiting the same production procedure: thanks to this it will be possible to compare the two material performances and then highlight the large grain material features. Among them, the potential benefits due to higher achievable thermal stability coming from the phonon peak around 2 K in thermal conductivity and the cost benefit due to lower bare material prices and simplified Nb fabrication process [5].

In this article, we present our experience on the material preparation, fabrication, treatments and testing of the LG niobium cavity based on our design for ESS Medium Beta cavities and some considerations about cavity performance.

## MATERIAL PREPARATION

CBMM (Brazil) produced a high RRR (≈ 300) Large Grain Nb ingot with a diameter compatible with the Medium Beta and High Beta ESS Superconducting cavities (about 480 mm), by using a special crucible and metallurgic techniques. This is nowadays the biggest LG Nb ingot ever produced. From this, two shorter and lighter ingots (about 200 kg) have been then obtained. Figure 1 shows the two ingots at Heraeus in preparation for the slicing process, just after their arrival from CBMM.

Figure 1: CBMM Large Grain ingots at Heraeus in preparation for the slicing process.

Heraeus GmbH in Hanau sliced then the ingot into disks with a 4.65 mm thickness using a multi-wire sawing machine adapted to our large ingot diameter. The "oxygen protection" technique has been employed so to avoid permanent degradation of RRR, by reducing $O_2$ diffusion and gettering. In Fig. 2 the LG disks after slicing process are shown.

Figure 2: Large Grain ingots after slicing at Heraus.

After the slicing process, the Nb sheets have been chemically etched by Buffered Chemical Polishing (BCP 1:1:2) to remove about 30 μm of mechanically damaged surface layer.

In order to reduce the hydrogen content, which is expected to increase during the wire-saw and BCP opera-

† Michele.bertucci@mi.infn.it
* now at ESS, Lund

ISBN: 978-3-95450-191-5 doi:10.18429/JACoW-SRF2017-TUPB046

tions, the Nb sheets were heat treated at 700 °C for 2 h in the Ultra High Vacuum furnace at Ettore Zanon S.p.A.

To cross check of all phases Nb samples, cut from the LG Nb disks, have been treated together with Nb disks and then analysed in terms of RRR and of the hydrogen content. RRR measurements have been done at LASA by means of an apparatus allowing to measure the resistivity of Nb samples at cryogenic temperatures, while the hydrogen content has been measured by means of a LECO machine at SAES Getters. Figure 3 shows the evolution of RRR and hydrogen content, measured by means of a LECO machine during the treatment steps.

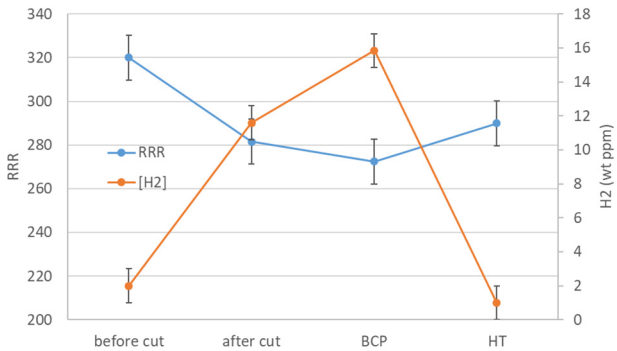


Figure 3: RRR and hydrogen content trend during treatments on Nb discs.

An evident change in RRR and hydrogen content can be noticed after disc cutting, and, as it can be expected, hydrogen concentration goes below 1 weight ppm after heat treatment. Anyway, no significant recovery of RRR takes place despite the successful hydrogen degassing. The scarce effect of hydrogen on RRR could be justified by appealing to a significant surface segregation [6].

## CAVITY FABRICATION

### *Subcomponents*

The cavity fabrication follows a standard procedure, which starts with Half Cells (HCs) deep drawing from Nb discs. Figure 4 shows one LG Nb disk ready for the deep-drawing operation.

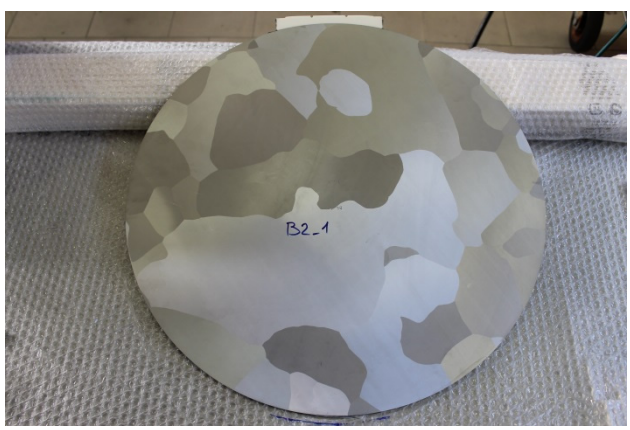


Figure 4: LG Nb disk ready for deep-drawing.

Then, the HCs are Electron Beam Welded (EBW) at the iris to form Dumb Bells (DBs). End Groups (EGs) are also prepared and then these components and the DBs are welded together to form the cavity. Details on the subcomponents fabrication and cavity composition are available in [3]. Figure 5 shows a Large Grain DB ready to be welded to form the cavity.

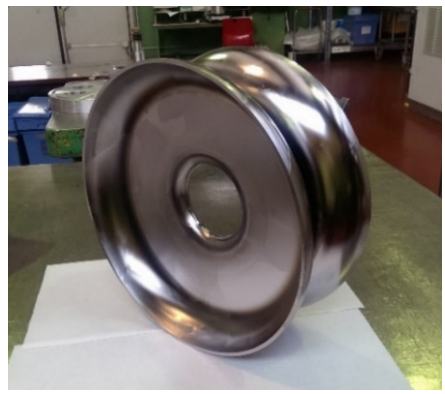

Figure 5: Large Grain dumb-bell ready to be welded to form the cavity.

The final goal is to reach the proper frequency and length of the cavity within the tolerances specified by ESS. For this, the DBs and the EGs are produced with extra metal to be trimmed to get final length and frequencies inside cavity specifications. As a peculiar feature of LG material, one must also take into account the dislocation of grain boundaries produced by mechanical stress, that contributes to modify the inner volume of the HC in a hard to control manner. This effect of grain boundaries on DB frequency is evident in Fig. 6, which shows the frequency spread versus dumbbell length. No correlation between length and frequency takes place, and this can be explained with the presence of large grain boundaries but also with the DB deformation during the trimming operation due to their large size.

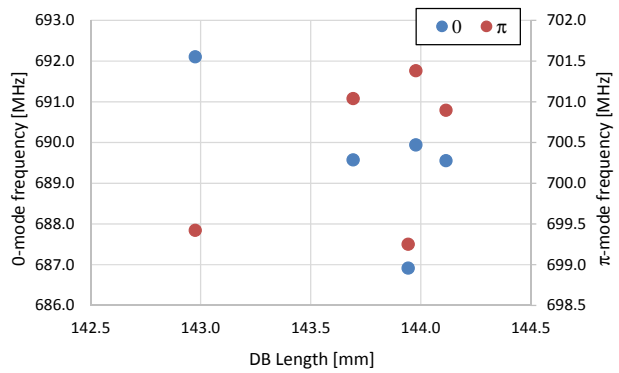


Figure 6: Distribution of 0-mode (blue dots) and π-mode (red dots) frequency versus Dumb Bell length.

### *Treatments*

The Large Grain cavity, after final equatorial EBW, has been then chemically treated with Bulk BCP to remove about 180 µm from the inner surface. To achieve a better removal uniformity, the Bulk BCP has been done in two

ISBN: 978-3-95450-191-5 doi:10.18429/JACoW-SRF2017-TUPB046

steps, flipping upside-down the cavity before each step. During this process, we monitored the temperature of the outer surface of the cell and observed an increase of the cell on the exit side of the acid up to 38 °C, while the acid temperature did not exceed 17.2 °C. A Nb sample is introduced inside the cavity volume through the main coupler in order to monitor the evolution of RRR. No significant variation of RRR is registered after each BCP step. Measurements on cavity thickness have been performed by means of ultrasonic thickness gauge so to check the homogeneity of thickness removal all along the cavity length.

The cavity is then heat treated at 600 °C for 10 hours, so to degas the hydrogen diffused during the previous chemical etching. Figure 7 shows the total pressure in the oven during the annealing process.

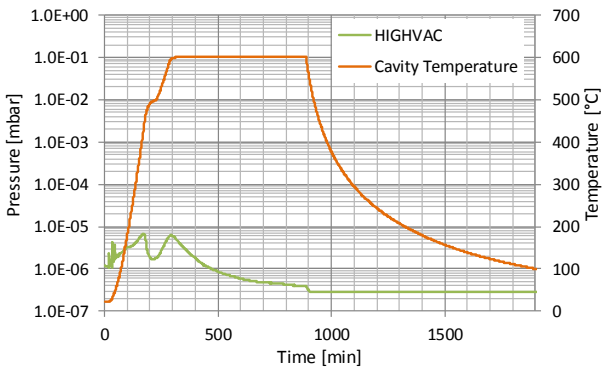


Figure 7: Pressure and temperature trend during the cavity heat treatment for dehydrogenation after Bulk BCP.

The choice of the 600 °C treatment temperature is motivated by the presence of Titanium components, since we want to avoid any pollution of the cavity surface and damage to Titanium parts due to higher temperature. The major contribution to the total pressure is hydrogen that is reduced by at least 20 times during the heat cycle. A final concentration of less than 1 weight ppm can be inferred from final pressure of $4 \cdot 10^{7}$ mbar [7].

### *Tuning*

After the heat treatment and before the final BCP treatment, the cavity has been tuned to the required frequency by a manual tuning machine exploiting the bead pull technique. The final field flatness is greater than 98% at the required frequency at warm at this stage of the preparation of 703.1 MHz [8].

Despite the before mentioned irregularities during Dumb Bell preparation, the cavity length turned out to be well within the required tolerances.

### *Final Preparation*

After the tuning, the cavity has been finally treated with a 20 µm BCP (Final BCP). The accessories assembly, i.e. the Pick Up and the Input Coupler antennas, was done in clean room and it was followed by a 12 h High Pressure Rinsing (HPR). After the installation of the UHV valve, the cavity was slow pumped and leak checked also recording the RGA to verify the vacuum quality. After the last RF spectrum, the cavity has been shipped to LASA for the cold test in vacuum.

## CAVITY TEST

The Large Grain cavity has been tested at LASA, in the upgraded Vertical Test Infrastructure.

The test facility is equipped with 20 second sound sensors installed on cavity frame, 11 fast-thermometry sensors placed on cavity surface and 4 PiN photodiodes for detecting X-ray radiation produced by field emission events. A proportional counter for external radiation dose measurement and a NaI scintillation detector for X-ray spectrum acquisition are placed above the cryostat top plate, along cavity axis. After the first FG cavity test [9], we went through a review of the facility so to reduce the magnetic field contribution to the residual resistance of the cavity. As an outcome of this activity, the maximum magnetic field has been reduced to 8 mG, in its turn corresponding to a maximum contribution of trapped magnetic flux to residual resistance of 2 nΩ. A further reduction of this value would require major modifications to the cryostat and insert that are planned in the near future.

### *First Test*

The Large Grain cavity has been tested in December 2016. Figure 8 shows Q vs $E_{acc}$ curve at 2 K for several tests, together with the radiation dose measured by the proportional counter.

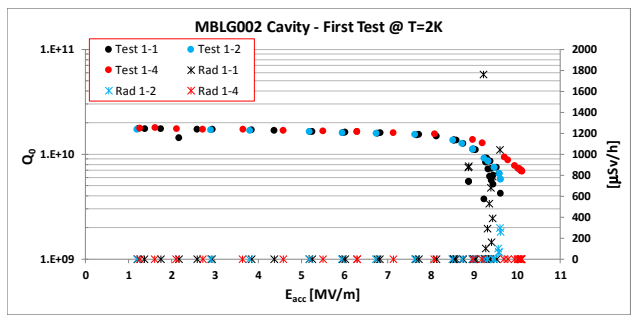


Figure 8: Q vs $E_{acc}$ for tests of the Large Grain cavity. Large radiation dose is observed in test 1-1.

The quality factor of the Large Grain cavity at low field is comparable with the one obtained for the Fine Grain cavity [8]. The cavity quenched just below 10 MV/m with a large radiation dose. We observed already a soft multipacting occurring at about 2 MV/m (as expected by simulation reported in [10]) clearly visible in a small drop of the $Q_0$ and in an increase in the emitted radiation. A second large increase of the radiation dose was then measured around 9 MV/m. The radiation dose was very high (up to 2 mSv/h), increasing exponentially with accelerating field until the cavity quench. Additional power rises at the all passband modes allow to reduce the emitted radiation dose by four orders of magnitude, but still at a higher value with respect to the Fine Grain cavity. The external X-ray spectrum is shown in Fig. 9, together with corresponding dose levels. The initial value of 5 MeV is fully

ISBN: 978-3-95450-191-5 doi:10.18429/JACoW-SRF2017-TUPB046

compatible with the results of CST and ASTRA simulations [11], giving at the nominal $E_{acc}$ of 10 MV/m a maximum impact energy of 4.9 MeV for electrons hitting the beam pipe flange. Endpoint energy reduces with conditioning, eventually stabilizing at 2.8 MeV. This suggests the presence of more field emitting sites on cavity surface: RF processing successfully eliminates the sites producing high energy electrons so drastically reducing the external dose level.

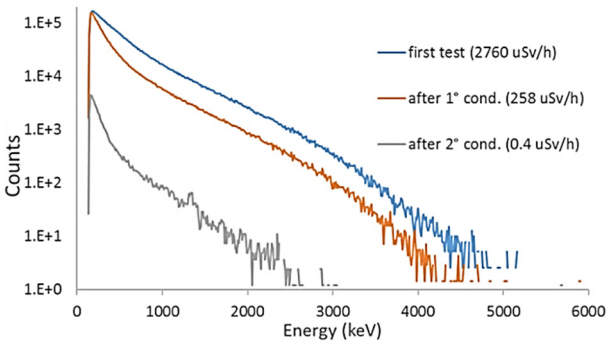


Figure 9: Scintillation spectra at quench field before and after conditioning. Acquisition time is 60 s. in all cases.

During all these measurement, the quench field instead did not change. Second sound analysis confirmed the occurrence of three different quench points. Figure 10 shows the reconstructed position for every pass-band mode, together with maximum $E_{acc}$ in quench cell.

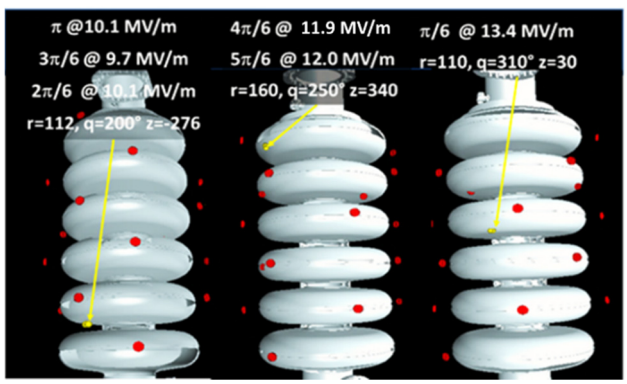


Figure 10: Second sound reconstruction of the 6 passband modes quench, gathered in "same quench" families.

The reconstructed mode profiles at quench field are reported in Table 1. The three quenching cells, as obtained by second sound, are marked with three different colours. As it can be seen, modal analysis is perfectly consistent with second sound results, since the cell field is always the maximum at quench. On the whole, a 13.4 MV/m maximum gradient is locally reached in π/6 mode. By means of optical inspection, some significant grain boundary structures are identified near the quench points, albeit not particularly prominent.

Table 1: cavity field profile in the 6 pass-band modes at quench field. The three different quench cells are marked with different colours.

| Max Eacc (MV/m) | 3.6 | 5.1 | 9.7 | 11.9 | 12.0 | 10.1 |
|---|---|---|---|---|---|---|

| Cell/mode | π/6 | 2π/6 | 3π/6 | 4π/6 | 5π/6 | π |
|---|---|---|---|---|---|---|
| 1 | 3.6 | 5.1 | 9.7 | **11.9** | **12.0** | 10.1 |
| 2 | 9.8 | 10.1 | 9.7 | 0.0 | 8.8 | 10.1 |
| 3 | **13.4** | 5.1 | 9.7 | 11.9 | 3.2 | 10.1 |
| 4 | 13.4 | 5.1 | 9.7 | 11.9 | 3.2 | 10.1 |
| 5 | 9.8 | **10.1** | **9.7** | 0.0 | 8.8 | **10.1** |
| 6 | 3.6 | 5.1 | 9.7 | 11.9 | 12.0 | 10.1 |

| Max E/mode (MV/m) | 13.4 | 10.1 | 9.7 | 11.9 | 12.0 | 10.1 |
|---|---|---|---|---|---|---|

Different scenarios could explain the low cavity performances: amongst them, electron dark current hitting cavity walls could produce enough heat to induce a thermal breakdown. Aiming to exclude (or confirm) this hypothesis, we proceeded with an additional 20 µm BCP and a longer 24-h HPR.

### *Second Test*

The cavity was tested the second time in April 2017. Figure 11 reports on the results obtained in the fundamental mode at different temperature of the LHe bath.

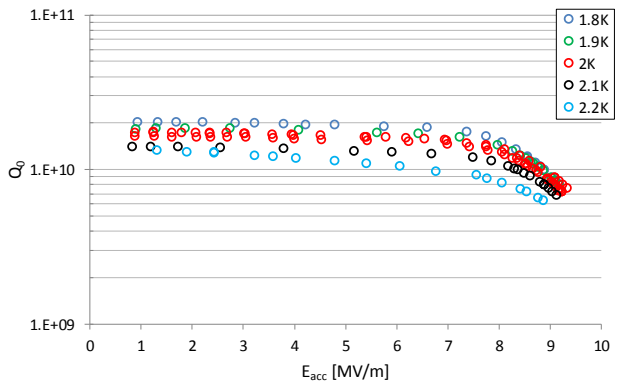


Figure 11: Large Grain cavity power rises at different temperature at the fundamental frequency.

As for the previous test, the $Q_0$ at low field was in the low $10^{10}$ range. Unlike the previous test, the radiation dose was in the background level and hence not measurable, cured by the light BCP and the 24 h HPR. Nevertheless, as for the first test the cavity quenched just above 9 MV/m at all the different temperatures. The difference in quench fields between the different LHe bath temperatures suggests a limitation of dissipated power at about 25 W, well below the cryogenic capacity of our plant set at about 40 W at 2 K. Mode analysis and Second sound confirmed exactly same quenching points of the first tests in all the pass-band modes.

This leads us to the conclusion that cavity performance limitation is due to thermal breakdown. After all, the fact

ISBN: 978-3-95450-191-5 doi:10.18429/JACoW-SRF2017-TUPB046



that no performance improvement is observed by varying test temperature lead us to conclude that no phonon peak improvement in LG Nb thermal conductance is present. This may be due to the low heat treatment temperature (600°C), which is not enough to release the mechanical stress of LG grains and recover the phonon mean free path-dependent term in thermal conductance [12]. Moreover, it is known that BCP treatment can increase the step size on grain boundaries [13], so increasing local magnetic field enhancement and then lowering the threshold for thermal breakdown. These two issues, maybe combined, can be responsible for low-field cavity quench.

Moreover, the analysis on material composition (RRR and hydrogen content) lead us to suspect a possible near-surface segregation of interstitials which can critically affect the cavity performances, for instance producing a premature flux penetration or modifying material parameters on the RF surface. Aiming to get more insight on the surface enriched layer, nuclear techniques for impurity depth profile, like Elastic Recoil Detection (ERD) and Rutherford Backscattering (RBS) will be employed in the next future on niobium samples with different treatment conditions (after cut, after BCP, after heat treatment).

## CONCLUSIONS

We produced and tested a Medium Beta Large Grain cavity prototype based on INFN-LASA designed developed for ESS.

The main difference with respect to the Fine Grain cavity prototype in the fabrication phase was in the RF characterization of components and the response to trimming operation. Instead, during all mechanical, welding and treatment operations the behaviour was similar to the Fine Grain one.

The low field quench during the power rise is still under analysis. We have not noticed a major change in $Q_0$ slope at different temperatures, indication that we did not enhanced the phonon peak possibly due to the low heat treatment temperature. The large radiation dose measured during the first test was clearly cured with a second Final BCP (~20 μm) BCP and a 24 h HPR.

The reasons of the premature quench at low field are still not clear. Based on our measurement evidence, the mechanism seems to be a few spots quenching at similar accelerating field. The power limit at about 25 W might be due either to low thermal conductance of the Nb sheets or to a bad heat transfer between the cavity and the LHe bath. These hypotheses are under investigation as well as analysis of the data acquired so far.

## REFERENCES

[1] P. Michelato *et al.*, "INFN Milano – LASA Activities for ESS", in *Proc. SRF2015*, Whistler, BC, Canada, 2015, THPB010.

[2] C. Darve *et al.*, "ESS Superconducting RF Collaboration", in *Proc. IPAC'17*, Copenhagen, Denmark, May 2017, MOPVA090.

[3] L. Monaco *et al.*, "Fabrication and Treatment of the ESS Medium Beta Prototype Cavities", in *Proc. IPAC'17*, Copenhagen, Denmark, May 2017, MOPVA060.

[4] D. Sertore *et al.*, "Experience on Design, Fabrication and Testing of a Large grain ESS", in *Proc. IPAC'17*, Copenhagen, Denmark, May 2017, MOPVA068.

[5] P. Kneisel *et al.*, "Progress on Large Grain and Single Grain Niobium–Ingots and Sheet and Review of Progress on Large Grain and Single Grain Niobium Cavities", in *Proc. SRF2007*, Beijing, China, TH102.

[6] A. Romanenko *et al*., "Elastic recoil detection studies of near-surface hydrogen in cavity-grade niobium", in *Supercond. Sci, Technol*., vol. 24, p. 105017 (2011).

[7] C. K Gupta, A. K Suri, *Extractive Metallurgy of Niobium*, p. 214, CRC press, Boca Raton, 1994.

[8] D. Sertore *et al.*, "INFN- LASA Medium Beta Cavity Prototypes for ESS Linac", presented at *SRF'17*, TUPB048, this conference.

[9] A. Bosotti *et al.*, "Vertical Tests of ESS Medium Beta Prototype Cavities at LASA", in *Proc. IPAC'17*, Copenhagen, Denmark, May 2017, MOPVA063.

[10] J. Chen *et al.*, "Multipacting Studies in ESS Medium-Beta Cavity", in *Proc. IPAC'17*, Copenhagen, Denmark, May 2017, MOPVA064.

[11] M. Bertucci *et al.*, "Quench and Field Emission Diagnostic for the ESS Medium Beta Prototypes Vertical Tests at LASA", in *Proc. IPAC'17*, Copenhagen, Denmark, May 2017, MOPVA061.

[12] P. Kneisel *et al.*," Review of ingot niobium as a material for superconducting radio frequency accelerating cavities", *Nucl. Instrum. Methods* A 774, p.133, 2015.

[13] W. Singer *et al.,* "Large-grain Superconducting RF Cavities at Desy", in *Proc. LINAC '06*, Knoxville, Tennessee USA, August 2006, TUP036.